



Article

Effect of Wall Proximity and Surface Tension on a Single Bubble Rising near a Vertical Wall

Raghav Mundhra¹, Rajaram Lakkaraju¹, Prasanta Kumar Das^{1,*}, Maksim A. Pakhomov² 
and Pavel D. Lobanov³ 

¹ Mechanical Engineering Department, Indian Institute of Technology, Kharagpur 721302, India

² Laboratory of Thermal and Gas Dynamics, Kutateladze Institute of Thermophysics SB RAS, 630090 Novosibirsk, Russia

³ Laboratory of Physical Hydrodynamics, Kutateladze Institute of Thermophysics SB RAS, 630090 Novosibirsk, Russia

* Correspondence: pkd@mech.iitkgp.ac.in

Abstract: Path instability of a rising bubble is a complex phenomenon. In many industrial applications, bubbles encounter walls, and the interactions between the bubbles and the wall have a significant impact on flow physics. A single bubble rising near a vertical wall was experimentally observed to follow a bouncing trajectory. To investigate the near-wall dynamics of rising bubbles, 3D numerical simulations were performed based on the volume of fluid (VOF) method using the open source solver OpenFOAM. The effect of wall proximity and surface tension on the bubble trajectory was investigated. Previous studies have focused on the near-wall rising dynamics of bubbles for higher Eotvos numbers (Eo) and varied the Galilei number (Ga). The physical properties of the flow were chosen such that the free-rising bubble lies in the rectilinear regime. The Ga number was fixed and the Eo number was varied to analyze its effect on the bubble's rising trajectory. It was found that the presence of the wall increases the drag experienced by the bubble and induces an early transition from rectilinear to a planar zigzagging regime. We identify the maximum wall distance and the critical Eo number for the bubble to follow a bouncing trajectory. The amplitude, frequency and wavelength of the bouncing motion are independent of the initial wall distance, but they decrease with decreasing surface tension.

Keywords: rising bubbles; path instability; wall effect; bouncing bubbles



Citation: Mundhra, R.; Lakkaraju, R.; Das, P.K.; Pakhomov, M.A.; Lobanov, P.D. Effect of Wall Proximity and Surface Tension on a Single Bubble Rising near a Vertical Wall. *Water* **2023**, *15*, 1567. <https://doi.org/10.3390/w15081567>

Academic Editor: Giuseppe Pezzinga

Received: 1 March 2023

Revised: 2 April 2023

Accepted: 14 April 2023

Published: 17 April 2023



Copyright: © 2023 by the authors. Licensee MDPI, Basel, Switzerland. This article is an open access article distributed under the terms and conditions of the Creative Commons Attribution (CC BY) license (<https://creativecommons.org/licenses/by/4.0/>).

1. Introduction

Rising bubbles have been a topic of active research due to their rich physics and various applications in different domains of science and engineering. Bubble behavior has a significant impact on the flow properties and heat and mass transfer effects in gas–liquid two-phase flows encountered in industry and many natural phenomena. The application domain of bubbles is very wide, ranging from heat exchangers and bubble column reactors to targeted drug delivery and laser histotripsy.

The non-linearity and the number of parameters involved make the dynamics of rising bubbles quite complex. The dynamics of a single bubble rising due to buoyancy in an infinite liquid pool has been the focus of many experimental [1–6] and numerical studies [7–14] in the past. A bubble can show different shapes and rising trajectories depending on the interplay between surface tension, viscosity and inertia forces. The contamination of the bubble surface can alter its dynamics in a significant manner [4].

In clean water, small bubbles follow a straight vertical path maintaining a spherical shape. There are no vortices behind the bubble making the flow axisymmetric. As the bubble size increases, it rises following a plane zigzag or a three-dimensional helical path. The fascinating phenomenon of path instability of a rising bubble has been the focus of many experimental, numerical [8] and analytical studies [15]. The transition from the

rectilinear to the oscillatory regime takes place when the streamwise vorticity accumulated on the bubble surface exceeds a critical value [5,16], resulting in an asymmetry in the vortical structures in the wake. The wake structures and vortical activity for the different path regimes have been extensively researched and documented [3,8,17]. Moreover, the bubbles also show significant shape deformations resulting in ellipsoidal, oblate ellipsoidal or cap shapes [4]. The shape deformations and wake instability have been considered responsible for the bubble path instability [12,18].

Gumulya et al. [19] and Senapati et al. [20] performed numerical simulations to investigate the effect of the bubble wake on a trailing bubble. They found that the leading bubble is unaffected by the proximity of the trailing bubble. The trailing bubble interacts with the wake of the leading bubble and accelerates. The path of the trailing bubble is also affected by the vorticity in the wake and the path deviation depends on the Reynolds and Eotvos numbers. Ghosh et al. [11] numerically modeled the shape distortion of one bubble due to the influence of the other and their merging.

In many industrial applications, bubbles encounter walls, and the interactions between the bubbles and the wall have a significant impact on flow physics. A single bubble rising near a vertical wall has been experimentally observed to follow a “bouncing” trajectory. Tsao and Koch [21] made observations for a single bubble rising very close to a wall at different inclination angles. They were the first to report that the bubble shows a steady bouncing behavior as it rises along the wall. After a certain critical angle, the bubble just slides along the wall. They linked this behavior to the bubble deformation dynamics. De Vries et al. [3] conducted experiments for a bubble rising very close to a vertical wall in still water. They observed that the bubble showed different behaviors such as sliding away, bouncing with constant amplitude or bouncing with increasing amplitude as the bubble size increases. Other researchers have explained this phenomenon based on the wall-induced lift force [22,23]. Podvin et al. [24] attempted to mathematically model the phenomenon using lubrication theory to model the wall-induced force. However, their model could not capture the bouncing process. Jeong and Park [25] carried out experimental studies for a high Re bubble rising at different distances from a vertical wall made of different materials. Lee and Park [26] suggested that the presence of the wall surface induces vortex shedding. Barbosa et al. [27] conducted experiments for a wide range of Reynolds and Weber numbers for bubbles rising near inclined walls. Using a force balance approach correlated with their experimental data, they formulated a condition for the critical angle for the transition from bouncing to sliding behavior.

The physics of this phenomenon is quite complex, and the mechanism of bouncing depends on several parameters. The problem of a rising bubble depends on four non-dimensional parameters:

Eotvos number-ratio of gravitational force to surface tension force $Eo = (\rho_l g d^2) / \sigma$

Galilei number-ratio of inertial force to viscous force $Ga = (\rho_l g^{1/2} d^{3/2}) / \mu_l$

Density ratio = ρ_l / ρ_g

Viscosity ratio = μ_l / μ_g

Here, ρ , μ , σ , d and g represent the density, dynamic viscosity, surface tension coefficient, bubble diameter and gravitational acceleration, respectively. The subscripts l and g denote the liquid and gas properties, respectively.

In an experimental setting, it is tough to independently vary the different parameters governing the phenomenon. Numerical simulations come in handy to explore physics incorporating a wider parameter space. Sugioka and Tsukada [28] investigated the drag and lift forces acting on an inviscid bubble moving near a plane wall using 3D direct numerical simulations. They found that, due to the presence of the wall, the drag force increases, and the direction of the lift force depends on the Reynolds number and the bubble-wall distance. Zhang et al. [29] simulated bubbles in the presence of a vertical wall and found that the amplitude and frequency of oscillatory bubble motion decrease with decreasing Galilei number. They also noted that the wall-normal dimensionless force, amplitude and frequency are almost independent of the wall-bubble initial distance. They predicted a

critical Galilei number for the transition from a steady to an oscillating regime, and it is found to be less than that for the unbounded condition. However, due to high Eo ($=16$), the bubble does not experience any attractive motion, and thus, bouncing motion and collision are not observed. Zhang et al. [30] performed 2D simulations for large deformable bubbles rising at different distances from the wall. They found that the bubble rises in a Z-shape and as the distance from the wall increases, the swing amplitude of the bubble gradually decreases, while the swing frequency of the bubble increases. Yan et al. [31] carried out VOF-based 3D simulations to investigate the bubble rising behavior near a vertical wall and observed the bubble bouncing motion. They found that as the Galileo number increases, the asymmetrical shedding of vortex structures is exacerbated by the presence of the wall. They predicted a critical Galilei number for the transition from rectilinear to spiral motion. The closer the bubble is to the wall, the earlier the transition occurs. Moreover, at low Galileo numbers, the bubble terminal velocity decreases due to the presence of the wall. Hasan and Hasan [32] studied the migration dynamics of an initially spherical bubble near a corner formed by two vertical walls and identified five regimes based on the bubble's migrating trajectory. Recently, Khodadadi et al. [33] performed numerical simulations over a wide range of Bond and Morton numbers for a single bubble rising near inclined walls. They identified three different bubble–wall interaction regimes—sliding, intermittent and non-contact—and plotted the regime map over the range of parameters considered.

The goal of this research is to explore the physics of bubble–wall interactions and gain insight into the bubble bouncing behavior as well as the parameters governing this phenomenon. The presence of a wall acts as a perturbation in the flow domain which can strongly affect the trajectory of the rising bubble and trigger the path instability of the bubble. For gas–liquid two-phase systems, a precise knowledge of the bubble trajectory is essential to estimate the gas-phase residence time through which the contact time for interfacial transport can be calculated. The bubble trajectory can be indirectly linked to the efficient design of gas–liquid two-phase systems. Moreover, knowledge of the parameters controlling the bubble trajectory can help us control the flow physics and heat transfer characteristics of many types of industrial equipment. Thus, a detailed investigation of the wall effect on the bubble dynamics is very much needed. This work focuses on the canonical case of a single bubble rising near a vertical wall which serves as the first step towards understanding multi-bubble systems encountered in industry.

Except for a few recent computational studies [28,30,31], the phenomenon of bouncing bubbles due to wall proximity has been studied in the past only through experiments. Experimental studies have their own constraints, and to delve deeper into the physics of any natural phenomenon, we need to look from the perspective of a wider parameter space. There is a need for a robust and well-established numerical model to capture this phenomenon. Moreover, there are still a lot of unanswered questions on bouncing bubbles, such as (1) which force plays the dominant role in governing the dynamics of bouncing; (2) how far into the liquid domain can the wall affect the bubble; (3) what is the role of the transport properties of both the fluids; (4) what are the kinematic and dynamic characteristics of the bouncing motion of the bubble, when observed in a wider parameter space; (5) a force balance model which can predict such dynamics.

To answer some of these questions, we use numerical simulations to analyze the effect of wall proximity and surface tension on the motion of a single bubble rising close to a vertical wall. In Section 2.2 we compare the parameter ranges covered in this work with the recent literature. Previous studies [25,29–31] have explored the effect of wall proximity on the dynamics of large bubbles with a higher Eotvos number. In this work, we study the effect of the initial bubble–wall distance on the dynamics of smaller bubbles with Eo and Ga corresponding to the air–water system. The bubble size is chosen such that the bubble lies in the rectilinear regime.

Tagawa et al. [34] explored the effect of surfactant concentration on the path instability of a bubble rising in a helical trajectory. For the case of bubbles rising near a vertical wall, previous works [29,31] have studied the effect of the Galilei number keeping the

Eotvos number fixed at values greater than 1. They predicted the critical Ga number for the transition from one regime to another. However, the authors have not come across any previous work studying the effect of the Eotvos number on bubbles rising near a vertical wall. Most of the previous research has focused on only discrete values of the Eu . In this work, by varying the surface tension, we systematically vary the Eotvos number over a large range (0.1–10) and find its critical value for the bubbles to start bouncing on the wall.

2. Computational Model

To study the wall effect on the rising motion of an initially spherical bubble, we initialize an air bubble of diameter d in a water tank of dimensions $(10d \times 60d \times 8d)$ (see Figure 1). The dimensions of the computational domain have been chosen as the bubble bouncing phenomenon while keeping the computational costs and time as low as possible.

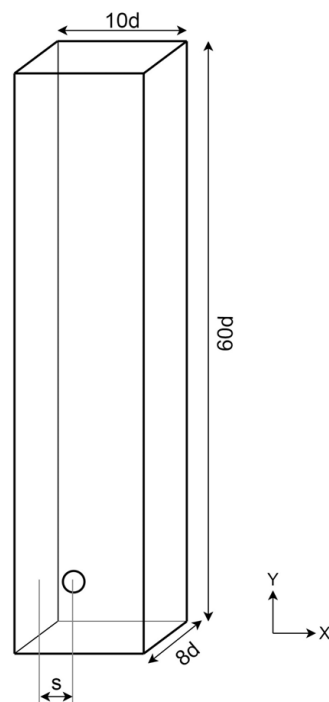


Figure 1. Schematic of the problem.

The height of the domain was taken as $60d$ so as to capture at least three bubble bounce events. Previous numerical studies [35] have shown that if the walls are at least $6d$ away from the bubble, then the computational domain can be treated as an unbounded fluid medium. The length and breadth have been taken as $10d$ and $8d$, respectively, so that there is no effect of the right wall, the front and back walls on the bubble motion. Since, the parameter range is chosen such that the bubble falls either in the rectilinear regime or the planar zigzagging regime and the bubble is going to bounce on the left wall (i.e., along the length of the domain) with negligible motion along the breadth of the domain, the length is kept greater than the breadth.

To avoid the influence of the right, bottom, back and front walls the initial co-ordinates of the bubble are set to $(s, 4d, 4d)$, where s is the normalized initial distance of the bubble centroid from the left wall. Thus, only the left wall would affect the dynamics of the bubble [35,36]. The initial bubble–wall distance has been normalized with respect to the bubble diameter.

The 3D computational simulation is performed with the interFoam solver in CFD code OpenFOAM, where the VOF model, is used to reconstruct the gas–liquid interface. OpenFOAM is a very robust open source CFD library and has been validated and used for the

study of bubble dynamics by many researchers [37–39]. The VOF method has been proven to be quite accurate to capture the physics of bubble–wall interactions [40,41].

2.1. Governing Equations and Numerical Model

The VOF model uses the phase fraction α to locate the phase interface. The grid cell is filled with the liquid phase when $\alpha = 1$, and when $\alpha = 0$, it is filled with the gas phase. The interface can be located as the region where α lies between 0 and 1.

The conventional VOF method involves the simultaneous solution of the continuity and momentum equations along with the solution of the transport equation for the phase fraction.

The incompressible continuity equation can be written as:

$$\nabla \cdot \mathbf{u} = 0 \quad (1)$$

The two phases share a common set of momentum equations, which can be represented as:

$$\frac{\partial \rho \mathbf{u}}{\partial t} + \nabla \cdot (\rho \mathbf{u} \mathbf{u}) = -\nabla p + \nabla \cdot \left[\mu \left(\nabla \mathbf{u} + \nabla \mathbf{u}^T \right) \right] + \mathbf{F}_\sigma + \rho \mathbf{g} \quad (2)$$

where \mathbf{u} represents the velocity vector shared by the two fluids throughout the flow domain. t and p denote the time and static pressure, respectively. \mathbf{F}_σ represents the surface tension force. In a single pressure system, the normal component of the pressure gradient at a stationary non-vertical solid wall with a no-slip condition must be different for each phase due to the hydrostatic component $\rho \mathbf{g}$ when the phases are separated at the wall. In order to simplify the definition of boundary conditions, a modified pressure is defined as:

$$p_d = p - \rho \mathbf{g} \cdot \mathbf{x} \quad (3)$$

where \mathbf{x} represents the position vector of the fluid element.

Using Equation (3) in (2) yields the modified momentum equation as follows:

$$\frac{\partial \rho \mathbf{u}}{\partial t} + \nabla \cdot (\rho \mathbf{u} \mathbf{u}) = -\nabla p_d - \mathbf{g} \cdot \mathbf{x} \nabla \rho + \nabla \cdot \left[\mu \left(\nabla \mathbf{u} + \nabla \mathbf{u}^T \right) \right] + \mathbf{F}_\sigma \quad (4)$$

Body forces due to pressure gradient and gravity are implicitly accounted for by the first two terms on the right-hand side of Equation (4).

In addition, the density ρ and viscosity μ are weighted by the phase fraction parameter as follows:

$$\rho = \alpha \rho_l + (1 - \alpha) \rho_g \quad (5)$$

$$\mu = \alpha \mu_l + (1 - \alpha) \mu_g \quad (6)$$

where α indicates the liquid phase fraction parameter. Subscripts l and g denote the liquid and gas phases, respectively.

The continuum surface force (CSF) model is used for surface tension. The surface tension force is calculated as follows:

$$\mathbf{F}_\sigma = \sigma \kappa \nabla \alpha \quad (7)$$

where σ represents the surface tension coefficient and κ represents the local curvature at the interface which can be approximated as follows:

$$\kappa = -\nabla \cdot \left(\frac{\nabla \alpha}{|\nabla \alpha|} \right) \quad (8)$$

In order to know where the interface between the two fluids is, an additional equation for α has to be solved:

$$\frac{\partial \alpha}{\partial t} + \nabla \cdot (\alpha \mathbf{u}) = 0 \quad (9)$$

In the interFoam solver, a two-fluid Eulerian formulation is used in which the phase fraction equation is solved separately for each individual phase [37].

$$\frac{\partial \alpha}{\partial t} + \nabla \cdot (\alpha \mathbf{u}_l) = 0 \quad (10)$$

$$\frac{\partial (1 - \alpha)}{\partial t} + \nabla \cdot ((1 - \alpha) \mathbf{u}_g) = 0 \quad (11)$$

The velocity is modeled in terms of the weighted average of the corresponding liquid and gas velocities as shown below:

$$\mathbf{u} = \alpha \mathbf{u}_l + (1 - \alpha) \mathbf{u}_g \quad (12)$$

Equations (10)–(12) can be combined [37] to obtain:

$$\frac{\partial \alpha}{\partial t} + \nabla \cdot (\alpha \mathbf{u}) + \nabla \cdot [\alpha (1 - \alpha) \mathbf{u}_C] = 0 \quad (13)$$

With this formulation, a sharper interface resolution is achieved. The phase fraction transport Equation (13) contains an extra convective term that is referred to as the compression term, which is used to keep the sharpness of the phase interface. In Equation (13), \mathbf{u}_C is called the compression velocity, which is, in essence, the relative velocity between the two phases. Since only a single velocity for both fluids is considered in the whole domain, the compression velocity needs to be modeled [37,38] as:

$$\mathbf{u}_C = c |\mathbf{u}| \left(\frac{\nabla \alpha}{|\nabla \alpha|} \right) \quad (14)$$

where c is the compression factor with the value of 1. Equation (14) closes the system of governing equations.

OpenFOAM solves the coupled system of Equations (1), (4) and (13) based on the finite volume method. The details of the used discretization schemes are given in Table 1. A predicted velocity field is constructed and then corrected repeatedly by using the pressure implicit with splitting of operators (PISO) iteration procedure. Details of the solution procedure followed by the solver can be found in this paper [38].

Table 1. Discretization schemes used for the different terms of the governing equations.

Term	Discretization Scheme	OpenFOAM Terminology
$\frac{\partial}{\partial t}(\rho \mathbf{u})$	Euler implicit time scheme	Euler
$\nabla \cdot (\rho \mathbf{u} \mathbf{u})$	Total Variation Diminishing	Limited linearV 1
$\nabla \cdot (\alpha \mathbf{u})$	Total Variation Diminishing	Gauss vanLeer
$\nabla \cdot [\alpha (1 - \alpha) \mathbf{u}_C]$	Bounded limited scheme	InterfaceCompression
$\nabla \cdot \mathbf{u}$	Central Differencing Scheme	Linear
$\nabla \alpha$	Central Differencing Scheme	Linear
$\nabla \cdot [\mu (\nabla \mathbf{u} + \nabla \mathbf{u}^T)]$	Central Differencing Scheme	Linear Corrected

All the walls were assigned a no-slip boundary condition for velocity and a zero gradient boundary condition for pressure. A static contact angle boundary [40] condition

was imposed on the left wall. Both the velocity and pressure fields were initialized as a uniform field with a value of zero.

The convergence tolerance was set to 1×10^{-6} for all the governing equations. The adjustable time step setting was turned on to ensure time step convergence.

The computations were performed on a supercomputing cluster using at least 128 cores in Intel Xeon SKL G-6148 processors running in parallel. Each solution needed at least 5 days of runtime.

2.2. Parameter Space

The density and viscosity ratios have been chosen to represent an air–water gas–liquid system. For the air–water system, taking $\rho = 1000 \text{ kg m}^{-3}$, $\mu = 0.001 \text{ Pa s}$, $g = 9.81 \text{ m s}^{-2}$ and $d = 0.001 \text{ m}$, we obtain $Ga = 99$. The case of $Ga = 99$ and $Eo = 0.14$ represent a 1 mm air bubble rising near a wall in pure water. Fixing the Ga and bubble diameter and varying the Eo from 0.1 to 10 allows us to study the effect of surface tension on the near-wall bubble behavior. In practical situations, we can control the surface tension of the air–water interface by using surfactants. These Eo values range can be considered as the value of Eo for a 1 mm air bubble rising in water having different surfactant concentrations. The knowledge of the effect of surface tension on the bubble behavior in water can be leveraged in practical situations to control the flow properties by using surfactants.

Table 2 shows a comparison between the parameters considered in previous research and this work. It is quite clear that we are exploring a parameter space that has been unexplored as of yet.

Table 2. Comparison of the range of physical parameters.

Researchers	Eo	Ga	s
Zhang et al. [29]	16	0.57, 63.36, 90.51	0.75, 1, 2
Yan et al. [31]	2	8.8, 51, 95, 133	0.75, 1, 2
Our work	0.1, 0.14, 1, 2, 10	99	0.75, 1, 1.2, 1.5

3. Results

To investigate the effect of a nearby vertical wall on the hydrodynamic behavior of a bubble, we divide this work into three parts. First, we compare the dynamics of a wall-bounded bubble with a free-rising bubble, then, we investigate the bubble dynamics at different initial wall distances. Finally, we study the effect of surface tension on the bubble behavior.

3.1. Grid Independence and Validation

We performed our simulations on a uniform mesh so as to obtain the same level of accuracy throughout the domain. To validate our model, we first chose a very coarse mesh with only 10 cells (see Figure 2a) across the bubble diameter. We then refined the mesh to obtain different meshes with 15 cells (see Figure 2b), 20 cells (see Figure 2c) and 25 cells across the bubble diameter. Simulations for an air bubble ($d = 1 \text{ mm}$) rising in pure water were performed using these meshes and the trend of rising velocity achieved by each mesh has been plotted in Figure 3. The results for terminal velocity for each mesh have been tabulated in Table 3. Figure 2d shows the mesh in the region between the bubble and the wall.

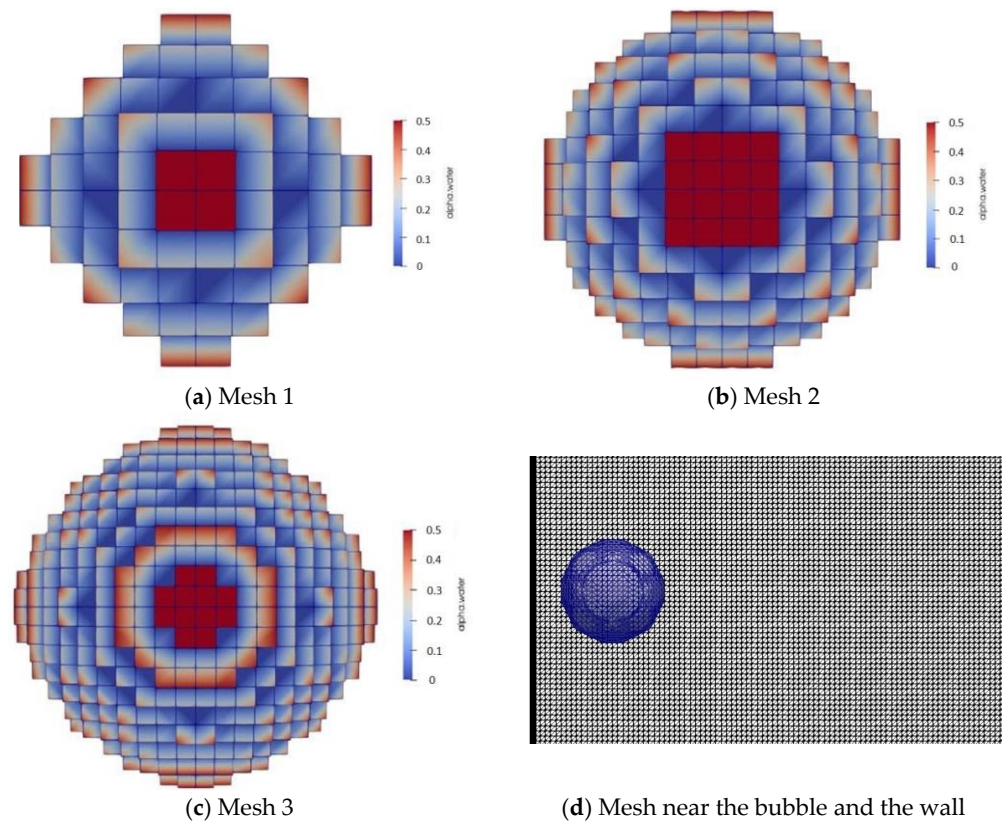


Figure 2. Bubble shape resolution for different meshes.

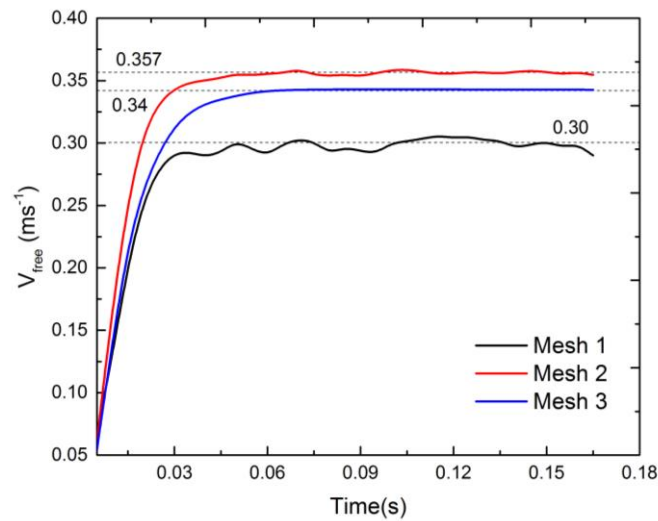


Figure 3. Bubble rise velocity for different meshes.

Table 3. Mesh refinement study.

Refinement Level	Number of Cells per Bubble Diameter	Terminal Velocity (m/s)
1	10	0.3
2	15	0.357
3	20	0.34

For simulating the phenomenon, a good resolution of the bubble surface is essential. It is quite clear from Figure 2a that Mesh 1 cannot resolve the bubble surface.

From Figure 3, we can see that the bubble velocity converges to a stable terminal velocity only for Mesh 3.

Mesh 4 (25 cells per bubble diameter) was also tested and there was not much difference in the results from Mesh 3. However, there was a considerable increase in the simulation time. Mesh 3 was thus the optimum choice for carrying out the simulations and the results from Mesh 3 can be considered to be grid independent.

The bubble terminal velocity for the same bubble size and fluid properties was calculated using the correlation of Jamialahmadi [42]. As can be seen from Table 4, the numerical results are in excellent agreement with the experimental correlation. The drag coefficient of the bubble is evaluated by balancing the buoyancy force and drag force at terminal conditions. The experimental drag coefficient for the same conditions has been obtained using Moore's correlation [4]. Both the numerical and experimental drag coefficients are shown in Table 4 below. The error between the experimental correlation and the numerical result is around 8%.

Table 4. Validation with experimental results.

	Numerical (Mesh 3)	Experimental	% Error
Terminal Velocity	0.34	0.344	1.16
Drag Coefficient	0.113	0.123	8.13

Thus, we can say that results from Mesh 3 are in agreement with experimental findings validating our model.

3.2. Near-Wall Rising Behaviour

For bubbles rising due to buoyancy, the near-wall bubble motion is very distinct from the motion of an unbounded bubble. Figure 4 shows the trajectory of a bubble ($d = 1$ mm, $Eu = 0.14$, $Ca = 99$) released at a distance of $s = 1, 4$ from the left wall. The bubble released at $s = 4$ shows a straight rising trajectory (Figure 4b) while the one released at $s = 1$ shows an almost two-dimensional zigzagging trajectory (Figure 4a). Since at $s = 4$ the rising trajectory is not affected by the wall, it can be considered an unbounded bubble.

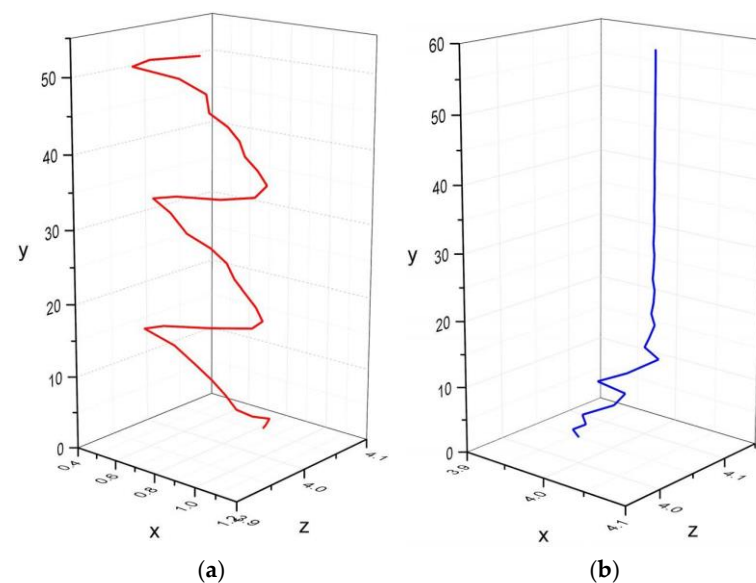


Figure 4. Comparison of the rising trajectory of a bubble released near a wall with that of an unbounded bubble: (a) 3D trajectory of the bubble released close to the wall; (b) 3D trajectory of the bubble released away from the wall. $d = 1$ mm, $Eu = 0.14$, $Ca = 99$.

It can be observed from Figure 5a that the unbounded bubble has no motion along the x -direction. However, the wall-bounded bubble shows a sinusoidal variation of its x -position with time, referred to as bouncing motion in the literature [3,21,25]. Figure 5b shows the variation of the wall-normal velocity for the wall-bounded and unbounded bubbles. After an initial transition state, the wall-normal velocity for the unbounded bubble converges to a steady value of zero, whereas the wall-normal velocity for the near-wall bubble shows a sinusoidal variation.

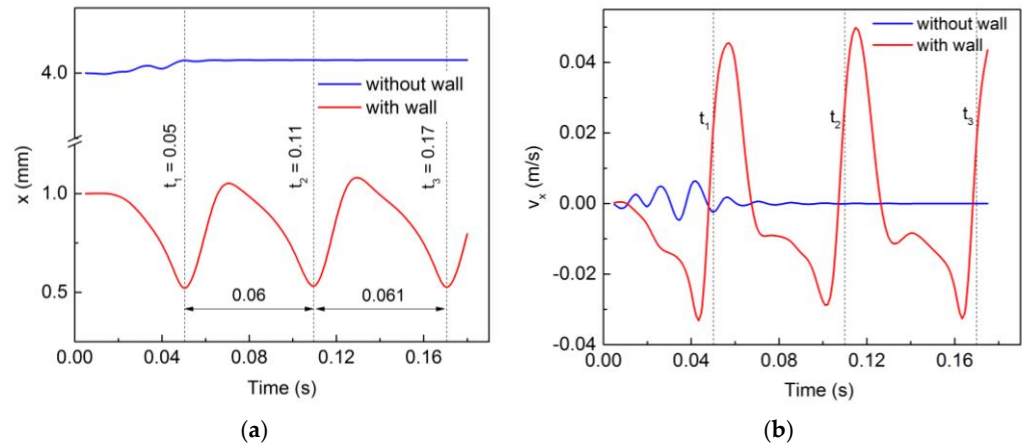


Figure 5. Comparison of x -motion of the bounded and unbounded bubble: (a) Time variation of x position of bubble centroid; (b) Time variation of x velocity of bubble centroid $d = 1$ mm, $Eu = 0.14$, $Ca = 99$.

The effect of the wall on the rising motion of the bubble is shown in Figure 6. The y -position of the bubble is monotonically increasing for both cases, but the slope for the bounded bubble is lesser than that for the unbounded bubble. The rise velocity of the wall-bounded bubble is fluctuating, and its terminal velocity is lower than that of the unbounded bubble.

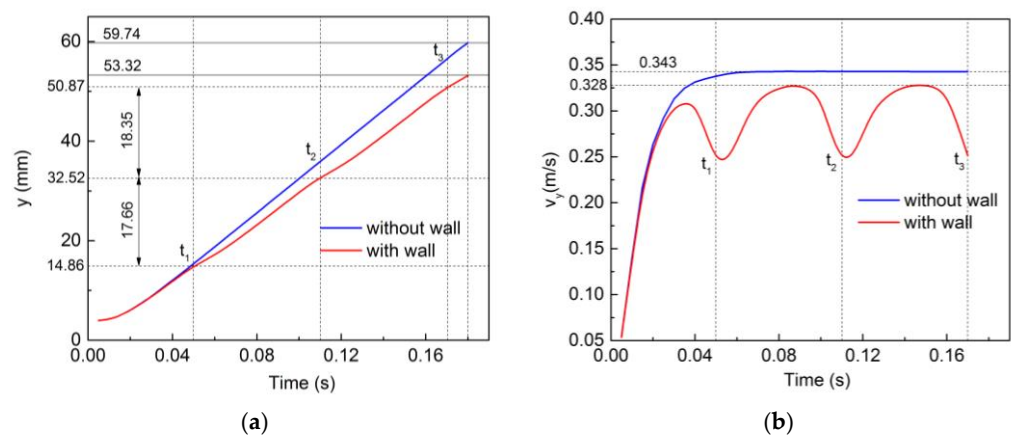


Figure 6. Comparison of y -motion of the bounded and unbounded bubble: (a) Time variation of y -position of bubble centroid; (b) Time variation of y -velocity of bubble centroid. $d = 1$ mm, $Eu = 0.14$, $Ca = 99$.

Now, if we look at the motion of the bubble in the spanwise direction (shown in Figure 7a,b) it is quite clear that the variations are of negligible magnitude compared to the variations in the other directions. For the unbounded bubble, after an initial transition state, the motion in the z -direction ceases and the z -position of the bubble gets fixed at $z = 4.05$ mm and z -velocity becomes zero. For the bounded bubble, random fluctuations in both the position and velocity in the z -direction are observed. However, the magnitude of these changes is very small.

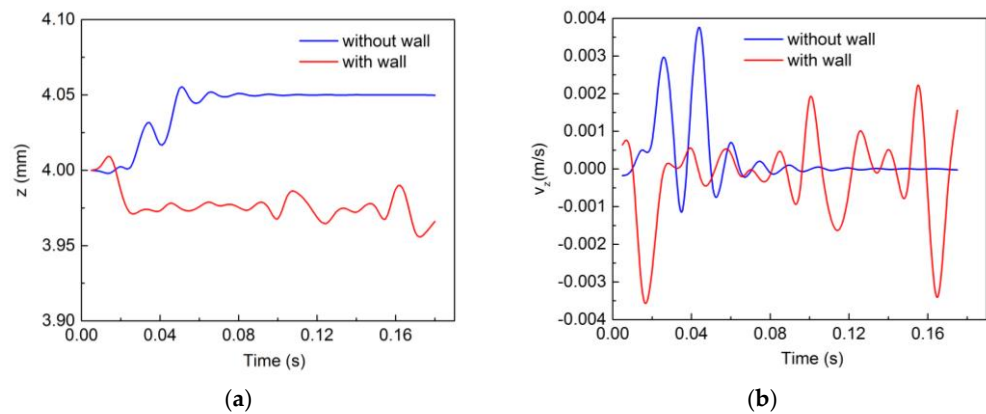


Figure 7. Comparison of z -motion of the bounded and unbounded bubble: (a) Time variation of z -position of bubble centroid; (b) Time variation of z -velocity of bubble centroid. $d = 1$ mm, $Eu = 0.14$, $Ca = 99$.

Figures 8 and 9 show the X and Y velocity contours, respectively, during a bounce event. It can be observed that just after the bubble–wall collision, both the x-velocity and the y-velocity in the region surrounding the bubble drop to significantly low values, thus breaking the continuity of the liquid flow around the bubble. This can be considered as the separation of the flow behind the bubble. It appears that the flow separation occurs after the bubble has bounced. This might have an effect on the wake region behind the bubble.

Figures 10 and 11 show the velocity vector plots around the wall-bounded and free bubble, respectively. It is clear that the wall provides a symmetry-breaking perturbation to the vortices in the flow field. As per Kelvin’s circulation theorem, vortices in the flow domain can generate lateral forces. From Figure 10, we can see that in the YZ plane, there are two symmetrical vortices in the wake of the bubble. The lateral force generated due to the two vortices on the bubble cancels out, and thus, the resultant force on the bubble is zero, resulting in no motion in the spanwise direction.

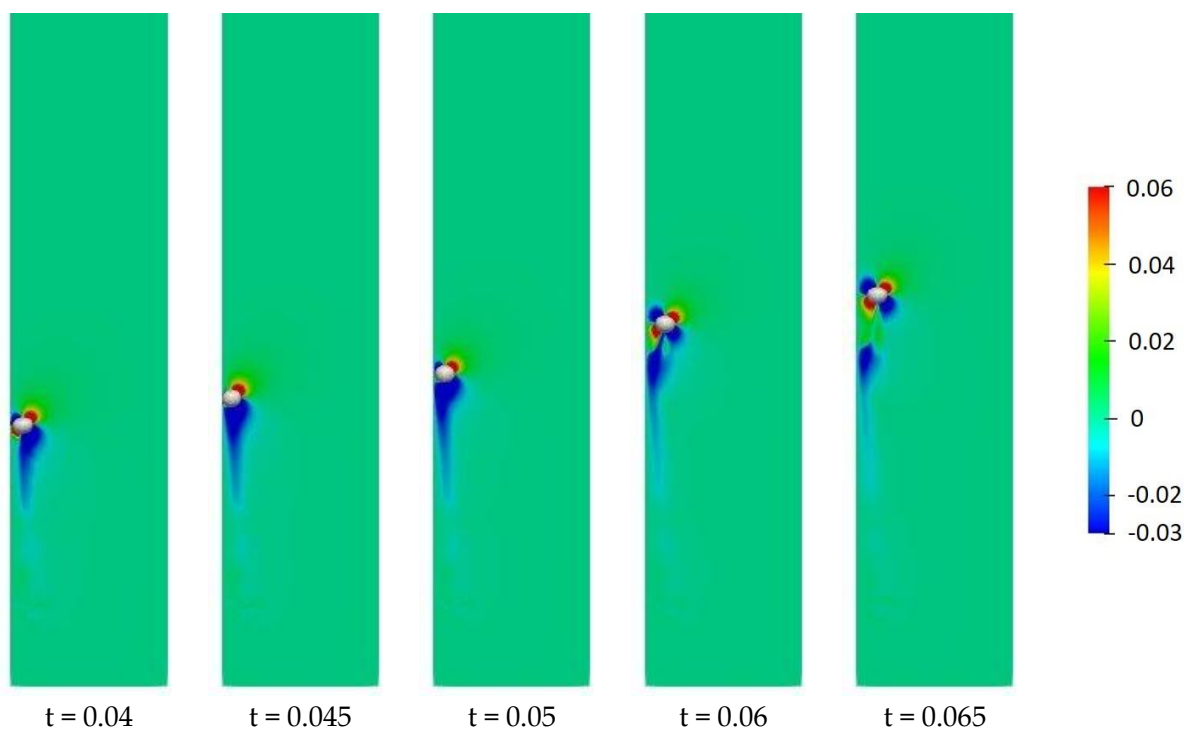


Figure 8. X-velocity contours during a bounce event ($s = 1$).

However, due to the presence of the wall, the flow structures in the XY plane become unsymmetrical. The vortex structures in the wake of the bubble are asymmetrical resulting in a net lateral force that attracts the bubble towards the wall. Thus, the asymmetry in the flow structures provides a qualitative explanation for the attractive lift force experienced by the bubble due to the presence of the wall. The bouncing phenomenon is just a consequence of this lift force. As the bubble rises near the wall, it is attracted towards the wall due to the lift force. When it becomes sufficiently close to the wall, the pressure in the thin liquid film between the bubble and the wall exerts a force that repels the bubble away from the wall. The bubble now moves away from the wall as it rises upwards. The lift force again attracts the bubble towards the wall while the pressure in the liquid film repels it. The amplitude of the bouncing motion, i.e., the maximum wall-normal distance reached by the bubble thus depends on the balance of these two forces. Moreover, the wavelength of the bouncing motion depends on the bubble rise velocity and the response time required for these two forces to balance out.

Now, for the case of a bubble rising away from the wall, the wake structures are symmetrical in both planes (Figure 11) and thus there is no net lateral force acting on the bubble and the bubble rises straight upwards following a rectilinear trajectory.

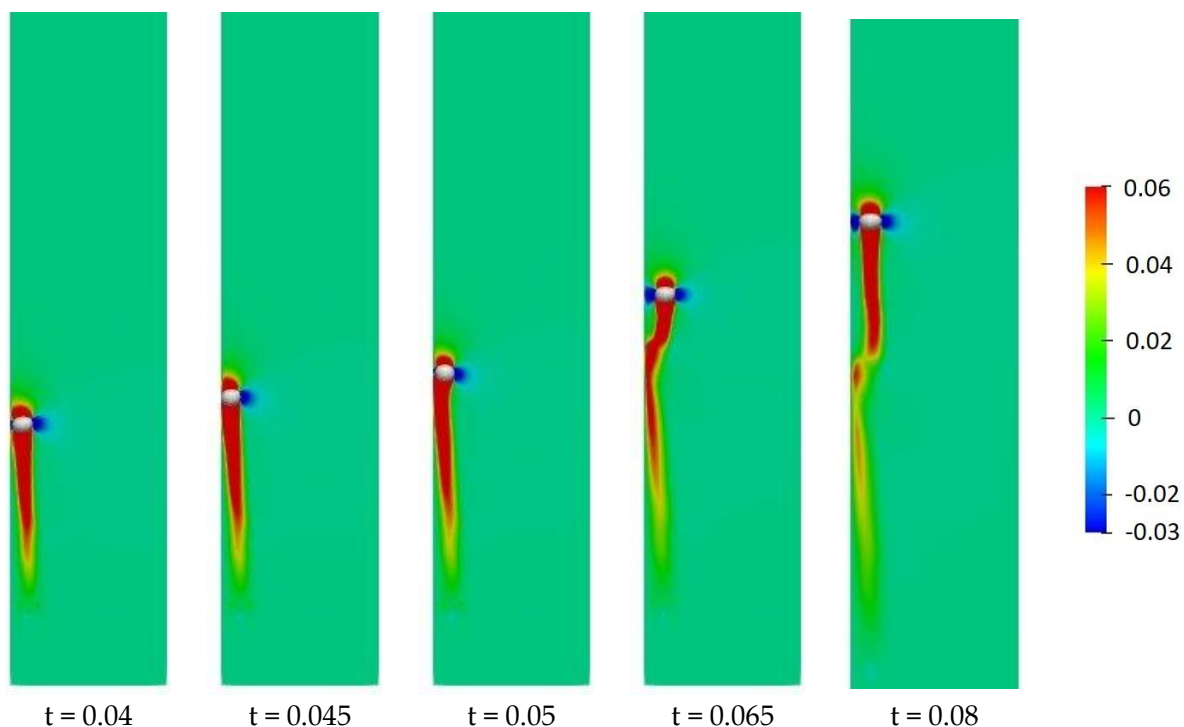


Figure 9. Y-velocity contours during a bounce event ($s = 1$).

3.3. Effect of Initial Wall Distance

To study the effect of the bubble–wall distance on the bubble rising behavior, we release the bubble at different distances from the wall. Keeping all other parameters fixed, we vary s as $s = 0.75, 1, 1.2, 1.5$. It is quite intuitive to expect the effect of the wall to decrease as the initial distance increases. This study will help us to analyze how far into the flow field the effect of the wall creeps in.

From Figure 12, we can see that as the bubble–wall initial distance increases, the bubble trajectory changes from bouncing to straight rising. The bubble shows a bouncing trajectory for s of less than 1.5.

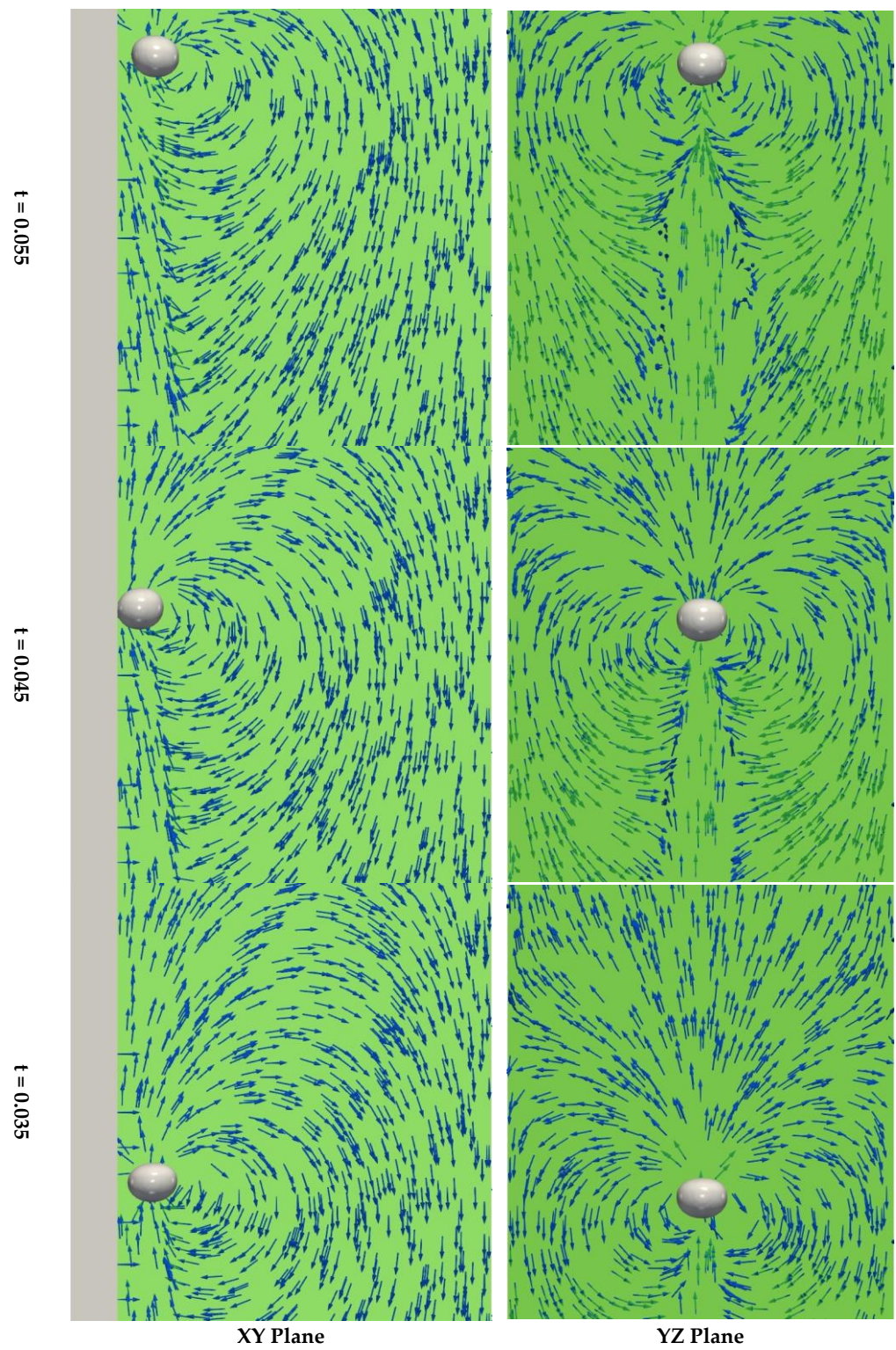


Figure 10. Velocity vector plots around a bubble rising close to the wall ($s = 1$).

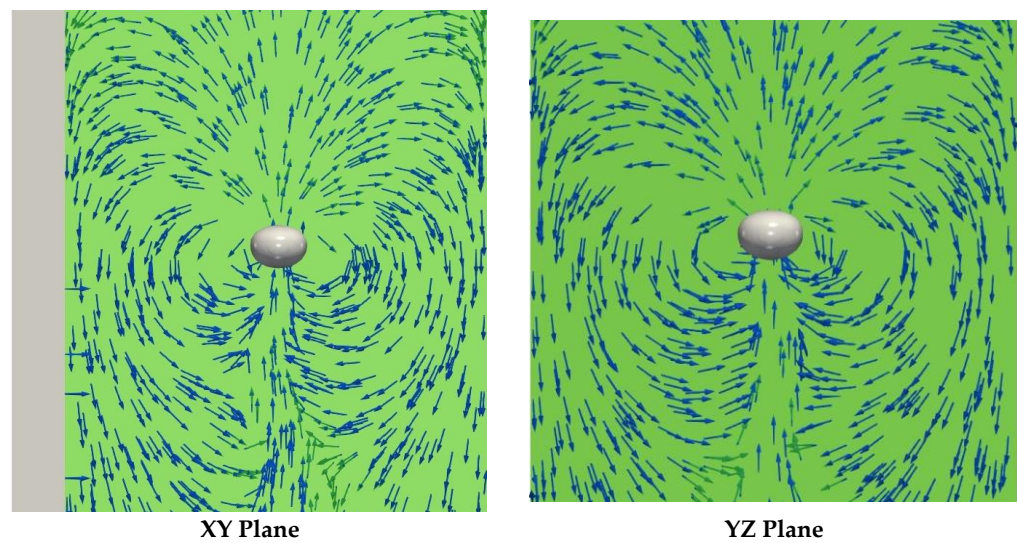


Figure 11. Velocity vector plot around a bubble rising away from the wall.

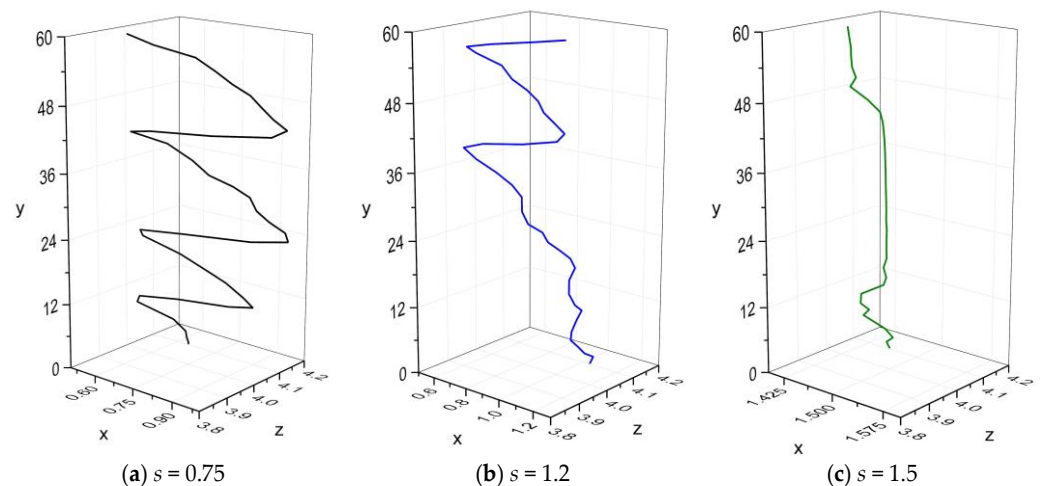


Figure 12. Comparison of the bubble trajectory when released at different distances from the wall ($Eo = 0.14$, $Ga = 99$).

Figure 13a,b shows the effect of the wall distance on the wall-normal motion of the bubble. The characteristics of the bouncing motion for different s are listed in Table 5. It is noted that for the s values for which the bubble shows a bouncing motion, the bouncing trajectory has almost similar characteristics. This implies that the initial wall distance does not impact the bouncing motion; however, there is just a phase difference of the bouncing trajectories (Figure 13a) for different s . In other words, as the distance from the wall increases, the time of onset of these instabilities also increases as we can observe for the cases of $s = 0.75, 1, 1.2$. After $s = 1.2$, the bubble does not show bouncing in the considered domain.

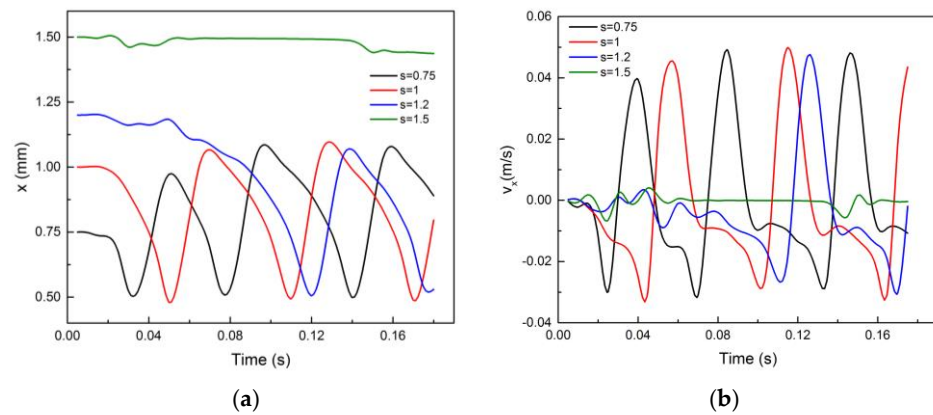


Figure 13. Comparison of x -motion of the bubble released at different distances from the wall: (a) Time variation of x -position of bubble centroid; (b) Time variation of x -velocity of bubble centroid. $d = 1$ mm, $Eo = 0.14$, $Ga = 99$.

Table 5. Characteristics of bouncing motion at different s ($Eo = 0.14$).

s	Amplitude (A) (mm)	Wavelength (λ) (mm)	Time Period (T) (s)
0.75	0.56	18.5	0.06
1	0.6	18	0.06

Figure 14a,b show the effect of the wall distance on the rising motion of the bubble. The rising velocity shows a fluctuating trend for s less than 1.5 and the terminal rise velocity decreases as s decreases.

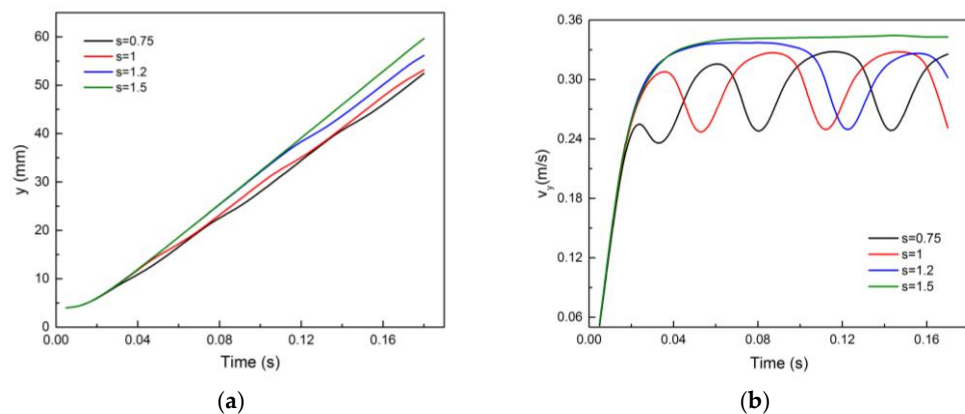


Figure 14. Comparison of y -motion of the bubble released at different distances from the wall: (a) Time variation of y -position of bubble centroid; (b) Time variation of y -velocity of bubble centroid. $d = 1$ mm, $Eo = 0.14$, $Ga = 99$.

Figure 15 below shows the variation of the average rise velocity of the bubble with the initial bubble–wall distance. As the wall proximity increases, the drag force on the bubble increases, and thus, the average rise velocity decreases. In terms of the drag force, $s = 1.5$ can be considered as the critical distance beyond which the wall has a negligible effect on the bubble motion.

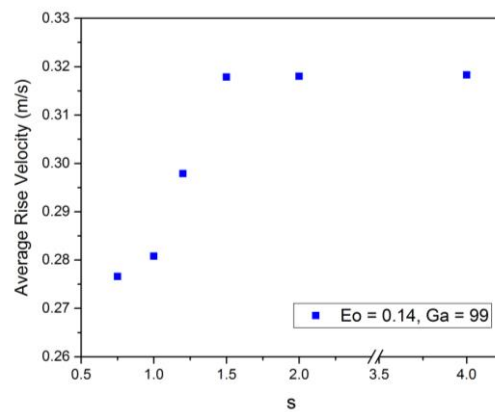


Figure 15. The variation of the average rise velocity of the bubble with initial wall distance.

As can be seen from Figure 16, the spanwise motion of the bubble is quite randomized.

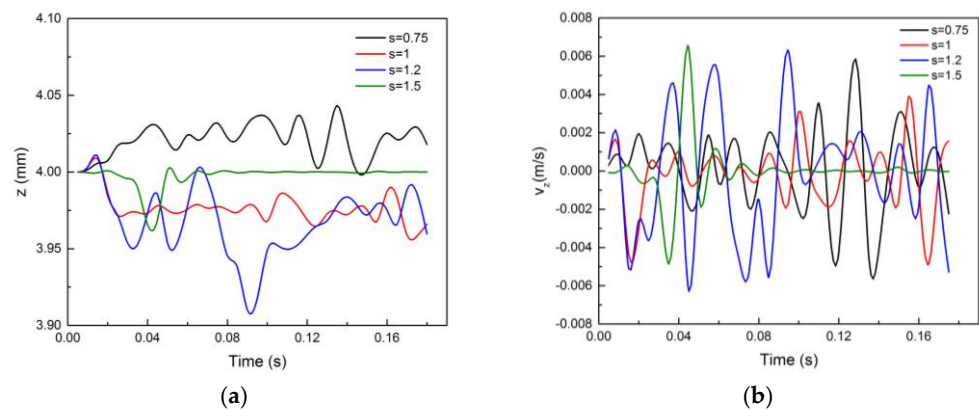


Figure 16. Comparison of z-motion of the bubble released at different distances from the wall: (a) Time variation of z-position of bubble centroid; (b) Time variation of z-velocity of bubble centroid. $d = 1$ mm, $Eo = 0.14$, $Ga = 99$.

However, the fluctuations in the z-component of velocity decrease as the distance from the wall increases. Moreover, the magnitude of the position variation and the velocity in spanwise direction is very small compared to the other two directions.

3.4. Effect of Surface Tension

Keeping the bubble size ($d = 1$ mm) and distance from the wall ($s = 1$) constant, we now vary the surface tension of the liquid–air interface. The different values of σ and the corresponding Eo are shown below (see Table 6):

Table 6. The Eotvos numbers vs. various surface tension coefficients.

σ	0.1	0.07	0.01	0.005	0.001
Eo	0.0981	0.14	0.981	1.96	9.81

Figure 17 shows how the bubble rising trajectory changes at different values of surface tension. After $Eo = 1$, the bubble shows a zigzagging trajectory while moving away from the wall.

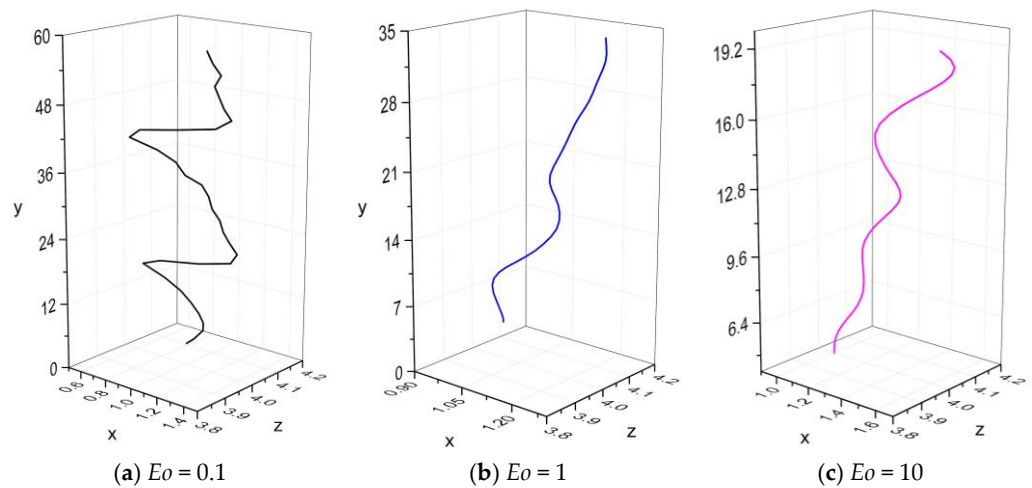


Figure 17. Comparison of the bubble trajectory at different Eo ($s = 1, Ga = 99$).

The effect of surface tension on the wall-normal motion, rising motion and spanwise motion is shown in Figures 18–21, respectively. It is evident from these figures that the wall effect on the bubble dynamics is dependent on the surface tension value. A detailed discussion of these results is performed in the following section.

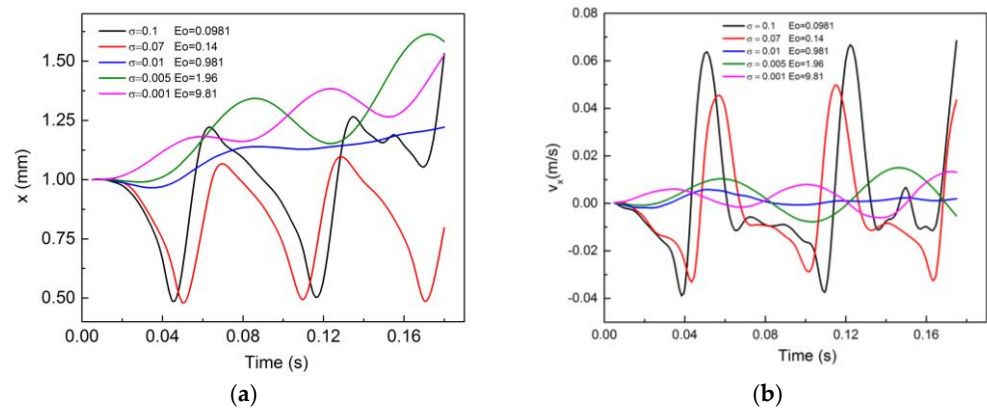


Figure 18. Comparison of x -motion of the bubble for different Eo : (a) Time variation of x -position of bubble centroid; (b) Time variation of x -velocity of bubble centroid. $d = 1$ mm, $Ga = 99, s = 1$.

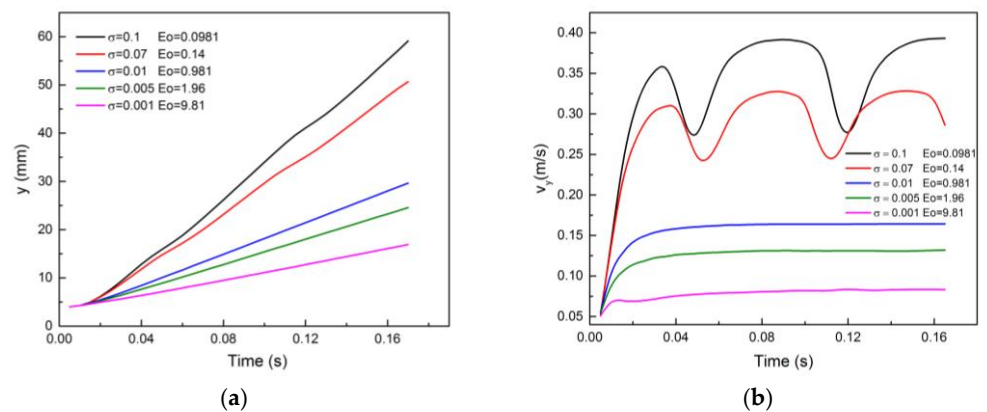


Figure 19. Comparison of y -motion of the bubble for different Eo : (a) Time variation of y -position of bubble centroid; (b) Time variation of y -velocity of bubble centroid. $d = 1$ mm, $Ga = 99, s = 1$.

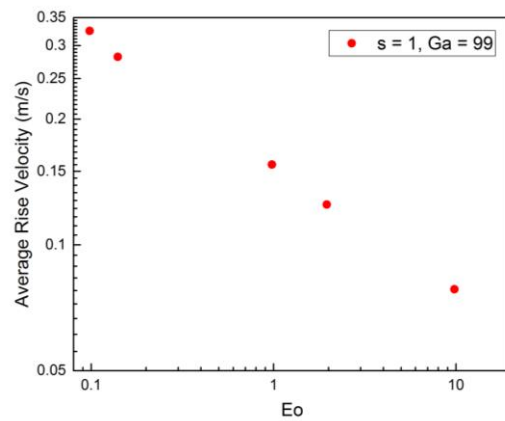


Figure 20. The variation of the average rise velocity of the bubble with Eotvos number.

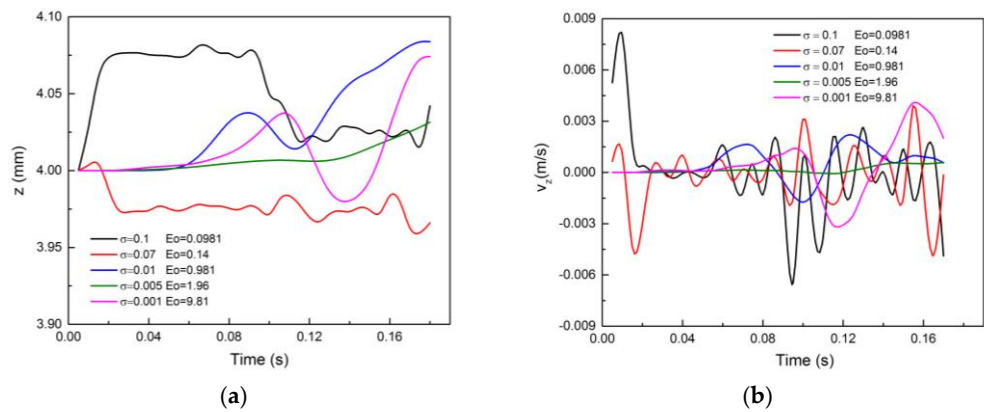


Figure 21. Comparison of z -motion of the bubble for different Eo : (a) Time variation of z -position of bubble centroid; (b) Time variation of z -velocity of bubble centroid. $d = 1$ mm, $Ga = 99$, $s = 1$.

From Table 7, we can see that for the values of surface tension for which the bubble shows a bouncing trajectory (Figure 18a), as the Eotvos number increases, the amplitude, time period and wavelength of the bouncing motion decreases.

Table 7. Characteristics of bouncing motion at different Eo ($s = 1$).

Eo	Amplitude (A) (mm)	Wavelength (λ) (mm)	Time Period (T) (s)
0.1	0.73	25.1	0.07
0.14	0.6	18	0.06

Figure 20 given below shows the variation of the average rise velocity of the bubble with the Eotvos number plotted on the log scale. It is evident from the plot that with increasing Eo , the rise velocity decreases. This implies that the decrease in surface tension indirectly increases the drag force.

From the above figure, we can observe that at lower surface tension values the bubble assumes a flat shape. Figure 22a,b shows the deformation in the bubble shape at the time of bouncing.

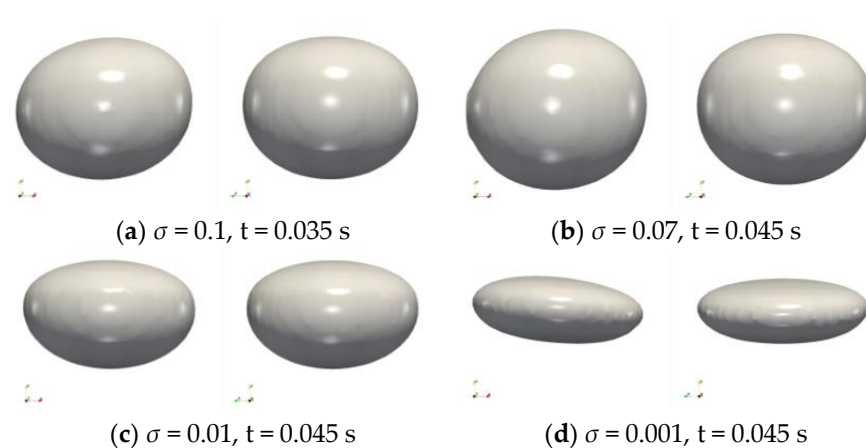


Figure 22. The bubble shape as viewed from the XY (left) and YZ (right) planes for different values of surface tension.

4. Discussion

According to phase diagram of Cano-Lozano et al. [13], a rising bubble with $Ga = 99$ and $EO = 0.14$ lies in the rectilinear regime. From Figure 4b, it is seen that the trajectory of the bubble far from the wall is straight rising. The wall proximity induces an early transition from the rectilinear to the planar zigzagging regime as shown in Figure 4a. This zigzagging motion on the wall is referred to as bouncing motion in the literature [21,25] as the bubble keeps on colliding with the wall, and thus, seems to bounce off the wall repeatedly.

From Figure 5, we can observe that the amplitude of this bouncing motion is constant. The bubble collides with the wall at t_1 , t_2 and t_3 . The time between two collisions is highlighted in the figure and is almost constant, i.e., the bouncing frequency is constant. The rising motion of the bounded and unbounded bubbles have the same nature (Figure 6). Figure 6 shows the vertical distance traveled by the wall-bounded bubble between two collisions (t_1, t_2) and (t_2, t_3) and it is almost constant. Thus, the bouncing motion is very uniform with constant amplitude, frequency and rise distance in every bouncing cycle.

On analyzing the x -component of the bubble velocity (Figure 5b), it is seen that the x -motion of the unbounded bubble has an initial transition state in which the x -velocity oscillates about the mean value of zero. After reaching the steady state, the x -motion ceases, i.e., x -velocity becomes zero. For the bounded bubble, the x -velocity shows a fluctuating trend. As expected, the velocity starts to rise at the time of the bubble–wall collision. From Figure 6a, it is evident that due to the presence of the wall, the drag force increases, and thus, the average rise velocity of the bounded bubble is lesser than that for the unbounded case.

As expected, the unbounded bubble reaches a terminal state with $v_y = 0.34$ m/s. However, the y -motion of the bounded bubble cannot achieve a steady state terminal velocity. After the buoyancy and drag forces are balanced, the bubble reaches a maximum $v_y = 0.32$ m/s. From Figures 5b and 6b, we can observe that at the time of the collision, the x -velocity starts increasing, and consequently, the y -velocity drops from its maximum value. As the bubble completes its bouncing cycle, the x -velocity decreases and the y -velocity starts rising and it again reaches its maximum value and stays there for some time after which the bubble is again attracted to the wall and the rising velocity drops again.

The spanwise motion (Figure 7a,b) is very negligible compared to those in the wall-normal and wall-parallel directions. However, compared to the unbounded bubble, there is some randomized motion in the spanwise direction for the bubble rising near the wall.

4.1. Effect of Wall Proximity

From Figures 12–15, it is evident that as s increases, the effect of the wall on the bubble decreases. For $s = 0.75$ and 1, the frequency and amplitude of bouncing are almost equal and constant (Table 5). However, there is a phase lag between them. For $s = 0.75$, the bubble is attracted towards the wall quite early as expected. As the distance from the wall increases,

it takes more time for the bubble to be attracted towards the wall. For $s = 1.2$, initially, the bubble rises straight upwards with negligible motion in the wall-normal direction. After $t = 0.15$, the bubble is attracted to the wall, and then after colliding with the wall, it shows a bouncing trajectory with almost the same amplitude and frequency as the previous cases. For $s = 1.5$, the bubble experiences negligible attraction towards the wall and its x -position decreases very slowly with time. At this distance, we can say that there is no effect of the wall, and hence, there is no bouncing motion. The wall-normal velocity shows a sinusoidal variation of constant amplitude and frequency, as expected for the bouncing motion. For $s = 1.2$ and 1.5 , the velocity shows small variations about zero, this is quite obvious as the bubble has no considerable motion in the x -direction.

The y -position of the bubble increases monotonically with an almost constant slope for all s . The slope of the line increases as s increases as observed in Figure 14a. As we can see from Figure 14b, the maximum y -velocity reached by the bubble increases as s increases. As the distance from the wall (s) increases, the drag force decreases, and thus, the average rise velocity increases. As explained in the previous section, the y -velocity magnitude shows a fluctuating pattern due to the bouncing motion. With increasing s , the bouncing motion dies out and so do the fluctuations in the y -velocity. As s increases, the maximum y -velocity achieved by the bubble increases. This is expected because, with increasing distance from the wall, the effect of the wall decreases, and thus, the effect of the wall on the rising velocity decreases. For $s = 1.5$, there are no fluctuations, and the rising velocity reaches a terminal state with $v_y \approx 1$. This implies that the terminal velocity is slightly lesser compared to the terminal velocity of the free-rising bubble. At $s = 1.5$, the wall effect is not strong enough to bring an effect in the wall-normal direction and induce a bouncing motion but it increases the drag, thus decreasing the y -velocity of the bubble.

4.2. Effect of Eotvos Number

Let us now analyze the effect of the variation of Eo on the bubble behavior. As the surface tension decreases and the Eo increases, the drag experienced by the bubble increases. This can be deduced from Figure 19. The y -position and the maximum rising velocity achieved decrease with increasing Eo number. This increase in drag can be attributed to the flattening of the bubble surface with decreasing surface tension.

At $Ga = 99$, the transition from rectilinear rising regime to planar zigzagging regime occurs at $Eo \approx 1.5$ [13]. In the presence of the wall, the bubble shows zigzagging motion (18a) for the entire range of Eo considered in this study, i.e., from $Eo = 0.098$ – 9.8 , except for $Eo = 1$. It is observed that for $Eo < 1$, the bubble bounces on the wall. Meanwhile, for $Eo > 1$, the bubble slowly moves away from the wall following a zigzagging trajectory. At $Eo = 1$, after an initial transition state, the bubble gradually slides away from the wall. Thus, at $Ga = 99$, $Eo = 1$ represents the critical value of Eo for which the wall force transitions from attractive to repulsive, thus changing the bubble motion from bouncing to sliding away.

For $Eo < 1$, with increasing surface tension and decreasing Eo , both the amplitude and the frequency of the bouncing motion increase (Figure 18a). The maximum wall-normal velocity achieved after the bubble–wall collision is also higher for lower Eo (Figure 18b). With regards to the motion in the spanwise direction, for the bouncing regime ($Eo < 1$) the oscillations of velocity in the z -direction increase with decreasing Eo , whereas for the sliding away regime ($Eo > 1$), the z -velocity magnitude is highest for the highest Eo . However, no particular trend can be fitted for the z -motion for any value of Eo and the order of magnitude of the velocity and displacement is negligible compared to those in the other two spatial directions.

5. Conclusions

In this work, VOF-based numerical simulations were performed to assess the impact of wall proximity and surface tension on the motion of a single air bubble rising in still water. For the parameters considered in this work, the bubble lies in the rectilinear regime. The following conclusions can be drawn from the obtained results:

- The presence of the wall near the bubble provides a significant perturbation to the flow structures in the fluid domain, which induces an early transition of the bubble trajectory from the rectilinear to the planar zigzagging regime. At $Ga = 99$, the critical Eo for this transition decreases from 1.5 to 0.14.
- A 1 mm diameter air bubble rising near a vertical wall in pure water ($Ga = 99, Eo = 0.14$) follows a bouncing trajectory as observed in previous experimental works. The bouncing motion is characterized by constant wavelength, amplitude and frequency. There is no significant motion of the bubble along the spanwise direction. The bouncing motion is thus two-dimensional.
- Due to the presence of the wall, the drag experienced by the bubble increases. The average rise velocity of the bubble rising near the wall is less compared to the unbounded bubble.
- As the bubble–wall initial distance increases, the bubble rising trajectory changes from bouncing (planar zigzagging) to straight rising. Moreover, as the distance from the wall increases, the maximum velocity and the average rise velocity also increases, i.e., the drag decreases.
- The bubble shows bouncing motion for $s < 1.5$. For the bouncing regime (i.e., $s < 1.5$), the change in wall proximity only changes the time of onset of bouncing. It does not impact the characteristics of the bouncing trajectory. The closer the bubble is to the wall, the earlier it triggers these path instabilities.
- For $Ga = 99, s = 1$, the bubble shows a bouncing motion for $Eo < 1$.

To have a complete picture of the effect of surface tension on the bubble bouncing behavior, the effect of wall proximity at different values of surface tension needs to be explored through more simulations in the future. Moreover, to further explore this phenomenon, the effect of bubble size on the bouncing motion should also be studied. Furthermore, well-planned experimental investigations should be conducted to supplement the computational study.

Author Contributions: Conceptualization, R.L., P.K.D., M.A.P. and P.D.L.; methodology, R.M., R.L. and P.K.D.; software, R.M.; validation, R.M.; formal analysis, R.M., R.L. and P.K.D.; investigation, R.M., R.L. and P.K.D.; resources, R.L. and P.K.D.; writing—original draft preparation, R.M.; writing—review and editing, R.L., P.K.D., M.A.P. and P.D.L.; supervision, R.L. and P.K.D.; project administration, R.L., P.K.D., M.A.P. and P.D.L.; funding acquisition, R.L., P.K.D., M.A.P. and P.D.L. All authors have read and agreed to the published version of the manuscript.

Funding: This research was funded by DST-RFBR through the project FLB.

Data Availability Statement: The data presented in this study can be made available on request.

Acknowledgments: The authors from India would like to acknowledge the support of National Supercomputing Mission (NSM) for providing HPC facility of PARAM Shakti at IIT Kharagpur, which is implemented by C-DAC and supported by the Ministry of Electronics and Information Technology (MeitY) and Department of Science and Technology (DST), Government of India. The co-authors from Russia are grateful to the state contract with IT SB RAS (Projects 121032200034-4 and 121031800217-8).

Conflicts of Interest: The authors declare no conflict of interest. The funders had no role in the design of the study; in the collection, analyses, or interpretation of data; in the writing of the manuscript; or in the decision to publish the results.

Abbreviations

The following abbreviations are used in this manuscript:

d	Bubble Diameter
Eo	Eotvos Number
g	Acceleration due to gravity
Ga	Galilei Number

s	Normalized bubble-wall initial distance
t	Time
v_x	x -velocity of bubble centroid
v_y	y -velocity of bubble centroid
v_z	z -velocity of bubble centroid
VOF	Volume of fluid
x	x -position of bubble centroid
y	y -position of bubble centroid
z	z -position of bubble centroid
α	Phase fraction
ρ	Density
σ	Surface Tension Coefficient
μ	Dynamic Viscosity

References

- Bhaga, D.; Weber, M.E. Bubbles in viscous liquids: Shapes, wakes and velocities. *J. Fluid Mech.* **1981**, *105*, 61. [\[CrossRef\]](#)
- Duineveld, P.C. The rise velocity and shape of bubbles in pure water at high Reynolds number. *J. Fluid Mech.* **1995**, *292*, 325–332. [\[CrossRef\]](#)
- Vries, A.W.D.; Biesheuvel, A.; Wijngaarden, L.V. Notes on the path and wake of a gas bubble rising in pure water. *Int. J. Multiph. Flow* **2003**, *28*, 1823–1835. [\[CrossRef\]](#)
- Clift, R.; Grace, J.R.; Weber, M.E. *Bubbles, Drops, and Particles*, 2nd ed.; Dover Publications: Mineola, NY, USA, 2005.
- Zenit, R.; Magnaudet, J. Path instability of rising spheroidal air bubbles: A shape-controlled process. *Phys. Fluids* **2008**, *20*, 061702. [\[CrossRef\]](#)
- Sharaf, D.M.; Premalata, A.R.; Tripathi, M.K.; Karri, B.; Sahu, K.C. Shapes and paths of an air bubble rising in quiescent liquids. *Phys. Fluids* **2017**, *29*, 122104. [\[CrossRef\]](#)
- Chen, L.; Garimella, S.V.; Reizes, J.A.; Leonardi, E. The development of a bubble rising in a viscous liquid. *J. Fluid Mech.* **1999**, *387*, 61–96. [\[CrossRef\]](#)
- Mougin, G.; Magnaudet, J. Path Instability of a Rising Bubble. *Phys. Rev. Lett.* **2001**, *88*, 014502. [\[CrossRef\]](#)
- Hua, J.; Lou, J. Numerical simulation of bubble rising in viscous liquid. *J. Comp. Phys.* **2007**, *222*, 769–795. [\[CrossRef\]](#)
- Farhangi, M.M.; Passandideh-Fard, M.; Moin, H. Numerical study of bubble rise and interaction in a viscous liquid. *Int. J. Comp. Fluid Dyn.* **2010**, *24*, 13–28. [\[CrossRef\]](#)
- Ghosh, S.; Das, A.K.; Vaidya, A.A.; Mishra, S.C.; Das, P.K. Numerical Study of Dynamics of Bubbles Using Lattice Boltzmann Method. *Ind. Eng. Chem. Res.* **2012**, *51*, 6364–6376. [\[CrossRef\]](#)
- Tripathi, M.K.; Sahu, K.C.; Govindarajan, R. Dynamics of an initially spherical bubble rising in quiescent liquid. *Nat. Commun.* **2015**, *6*, 6268. [\[CrossRef\]](#) [\[PubMed\]](#)
- Cano-Lozano, J.C.; Martínez-Bazán, C.; Magnaudet, J.; Tchoufag, J. Paths and wakes of deformable nearly spheroidal rising bubbles close to the transition to path instability. *Phys. Rev. Fluids* **2016**, *1*, 053604. [\[CrossRef\]](#)
- Gumulya, M.; Joshi, J.B.; Utikar, R.P.; Evans, G.M.; Pareek, V. Bubbles in viscous liquids: Time dependent behaviour and wake characteristics. *Chem. Eng. Sci.* **2016**, *144*, 298–309. [\[CrossRef\]](#)
- Shew, W.L.; Pinton, J.F. Dynamical Model of Bubble Path Instability. *Phys. Rev. Lett.* **2006**, *97*, 144508. [\[CrossRef\]](#)
- Ern, P.; Risso, F.; Fabre, D.; Magnaudet, J. Wake-Induced Oscillatory Paths of Bodies Freely Rising or Falling in Fluids. *Ann. Rev. Fluid Mech.* **2012**, *44*, 97–121. [\[CrossRef\]](#)
- Zenit, R.; Magnaudet, J. Measurements of the streamwise vorticity in the wake of an oscillating bubble. *Int. J. Multiph. Flow* **2009**, *35*, 195–203. [\[CrossRef\]](#)
- Magnaudet, J.; Eames, I. The Motion of High-Reynolds-Number Bubbles in Inhomogeneous Flows. *Annu. Rev. Fluid Mech.* **2000**, *32*, 659–708. [\[CrossRef\]](#)
- Gumulya, M.; Utikar, R.; Evans, G.; Joshi, J.; Pareek, V. Interaction of bubbles rising inline in quiescent liquid. *Chem. Eng. Sci.* **2017**, *166*, 1–10. [\[CrossRef\]](#)
- Senapati, A.; Singh, G.; Lakkaraju, R. Numerical simulations of an inline rising unequal-sized bubble pair in a liquid column. *Chem. Eng. Sci.* **2019**, *208*, 115159. [\[CrossRef\]](#)
- Tsao, H.K.; Koch, D.L. Observations of high Reynolds number bubbles interacting with a rigid wall. *Phys. Fluids* **1997**, *9*, 44–56. [\[CrossRef\]](#)
- Takemura, F.; Takagi, S.; Magnaudet, J.; Matsumoto, Y. Drag and lift forces on a bubble rising near a vertical wall in a viscous liquid. *J. Fluid Mech.* **2002**, *461*, 277–300. [\[CrossRef\]](#)
- Takemura, F.; Magnaudet, J. The transverse force on clean and contaminated bubbles rising near a vertical wall at moderate Reynolds number. *J. Fluid Mech.* **2003**, *495*, 235–253. [\[CrossRef\]](#)
- Podvin, B.; Khoja, S.; Moraga, F.; Attinger, D. Model and experimental visualizations of the interaction of a bubble with an inclined wall. *Chem. Eng. Sci.* **2008**, *63*, 1914–1928. [\[CrossRef\]](#)

25. Jeong, H.; Park, H. Near-wall rising behaviour of a deformable bubble at high Reynolds number. *J. Fluid Mech.* **2015**, *771*, 564–594. [[CrossRef](#)]
26. Lee, J.; Park, H. Wake structures behind an oscillating bubble rising close to a vertical wall. *Int. J. Multiph. Flow* **2017**, *91*, 225–242. [[CrossRef](#)]
27. Barbosa, C.; Legendre, D.; Zenit, R. Conditions for the sliding-bouncing transition for the interaction of a bubble with an inclined wall. *Phys. Rev. Fluids* **2016**, *1*, 032201. [[CrossRef](#)]
28. Sugioka, K.; Tsukada, T. Direct numerical simulations of drag and lift forces acting on a spherical bubble near a plane wall. *Int. J. Multiph. Flow* **2015**, *71*, 32–37. [[CrossRef](#)]
29. Zhang, Y.; Dabiri, S.; Chen, K.; You, Y. An initially spherical bubble rising near a vertical wall. *Int. J. Heat Fluid Flow* **2020**, *85*, 108649. [[CrossRef](#)]
30. Zhang, K.; Li, Y.; Chen, Q.; Lin, P. Numerical Study on the Rising Motion of Bubbles near the Wall. *Appl. Sci.* **2021**, *11*, 10918. [[CrossRef](#)]
31. Yan, H.; Zhang, H.; Liao, Y.; Zhang, H.; Zhou, P.; Liu, L. A single bubble rising in the vicinity of a vertical wall: A numerical study based on volume of fluid method. *Ocean Eng.* **2022**, *263*, 112379. [[CrossRef](#)]
32. Hasan, S.M.M.; Hasan, A.B.M.T. Migration dynamics of an initially spherical deformable bubble in the vicinity of a corner. *Phys. Fluids* **2022**, *34*, 112119. [[CrossRef](#)]
33. Khodadadi, S.; Samkhaniani, N.; Taleghani, M.H.; Bandpy, M.G.; Ganji, D.D. Numerical simulation of single bubble motion along inclined walls: A comprehensive map of outcomes. *Ocean Eng.* **2022**, *255*, 111478. [[CrossRef](#)]
34. Tagawa, Y.; Takagi, S.; Matsumoto, Y. Surfactant effect on path instability of a rising bubble. *J. Fluid Mech.* **2014**, *738*, 124–142. [[CrossRef](#)]
35. Mukundakrishnan, K.; Quan, S.; Eckmann, D.M.; Ayyaswamy, P.S. Numerical study of wall effects on buoyant gas-bubble rise in a liquid-filled finite cylinder. *Phys. Rev. E* **2007**, *76*, 036308. [[CrossRef](#)] [[PubMed](#)]
36. Krishna, R.; Urseanu, M.; van Baten, J.; Ellenberger, J. Wall effects on the rise of single gas bubbles in liquids. *Int. Comm. Heat Mass Transf.* **1999**, *26*, 781–790. [[CrossRef](#)]
37. Klostermann, J.; Schaake, K.; Schwarze, R. Numerical simulation of a single rising bubble by VOF with surface compression. *Int. J. Numer. Methods Fluids* **2013**, *71*, 960–982. [[CrossRef](#)]
38. Deshpande, S.S.; Anumolu, L.; Trujillo, M.F. Evaluating the performance of the two-phase flow solver interFoam. *Comp. Sci. Discov.* **2012**, *5*, 014016. [[CrossRef](#)]
39. Pradeep, A.; Sharma, A.K. Numerical investigation of single bubble dynamics in liquid sodium pool. *Sādhanā* **2019**, *44*, 56. [[CrossRef](#)]
40. Senthilkumar, S.; Delauré, Y.; Murray, D.; Donnelly, B. The effect of the VOF–CSF static contact angle boundary condition on the dynamics of sliding and bouncing ellipsoidal bubbles. *Int. J. Heat Fluid Flow* **2011**, *32*, 964–972. [[CrossRef](#)]
41. Albadawi, A.; Donoghue, D.; Robinson, A.; Murray, D.; Delauré, Y. On the assessment of a VOF based compressive interface capturing scheme for the analysis of bubble impact on and bounce from a flat horizontal surface. *Int. J. Multiph. Flow* **2014**, *65*, 82–97. [[CrossRef](#)]
42. Kulkarni, A.A.; Joshi, J.B. Bubble Formation and Bubble Rise Velocity in Gas–Liquid Systems: A Review. *Ind. Eng. Chem. Res.* **2005**, *44*, 5873–5931. [[CrossRef](#)]

Disclaimer/Publisher’s Note: The statements, opinions and data contained in all publications are solely those of the individual author(s) and contributor(s) and not of MDPI and/or the editor(s). MDPI and/or the editor(s) disclaim responsibility for any injury to people or property resulting from any ideas, methods, instructions or products referred to in the content.